Assessment of solid state and liquid phase sintering models by comparison of isothermal densification kinetics in W and W-Cu systems

Francis Delannay, Jean-Michel Missiaen

Assessment of solid state and liquid phase sintering models by comparison of isothermal densification kinetics in W and W-Cu systems

Francis Delannay[a], Jean-Michel Missiaen[b]

[a]Université catholique de Louvain, Institute of Mechanics, Materials and Civil Engineering, iMMC/IMAP, Place Sainte Barbe 2, B-1348 Louvain-la-Neuve, Belgium
[b]Université de Grenoble Alpes & CNRS, Laboratoire de Science et Ingenierie des Materiaux et Procedes, SIMAP, 101, rue de la Physique BP 46, F-38000 Grenoble, France

The role of liquid phase and grain growth during the intermediate stage of sintering is investigated by comparing the isothermal densification rate of the tungsten skeleton in two systems: solid-state sintered W and liquid-phase sintered W-10wt%Cu. Densification curves at 1380 °C, i.e. well after completion of capillary rearrangement in W-Cu, are confronted to the predictions of a model that considers a single representative grain size with quasi-equilibrium interfaces and a monotonic increase in grain size and coordination with density. In both systems, the densification mechanism is taken to be governed by W diffusion along grain boundaries. For system W-Cu, a phenomenological law is proposed to allow ac-counting for the decrease in liquid surface curvature during funicular filling of the pores by the liquid-phase. The kinetics of grain growth is described via current literature model. Good agreement is demonstrated between experimental measurements and model predictions when relying on material parameter values given in literature. In system W-Cu, the detrimental effect of the decrease in dihedral angle is, at the beginning of the funicular stage, compensated by the contribution to sintering stress brought about by the concave curvature of liquid/vapour interface. The sensitivity of computational results to model hypotheses and material parameters is assessed. The most influential parameters are diffusivities along W grain boundaries and along W/vapour and W/Cu interfaces.

1. Introduction

Microstructure-based models for the simulation of sintering kinetics embody the current understanding of basic phenomena underlying sintering. A step forward in microstructure-based modelling has been brought in a series of papers published in the nineties by the group of Riedel, Svoboda and co-workers [1–5]. Significant progresses along the same modelling approach have been contributed more recently by Wakai and co-workers [6–12]. Computational tools inspired by these models are available for practitioners of sintering technology [13]. Nevertheless, unlike the wealth of theoretical work, papers aiming at in-depth model assessment on the basis of experimental results are scarce [14].

Composites W-Cu arouse interest for potential application as materials for electrical contact or for thermal transfer management in fusion power plants [15–20]. Whereas pores contain only vapour in aggregates of pure W grains, they can contain both liquid and vapour in aggregates W-Cu. The kinetics of solid state sintering of W with and without addition of activator has been modelled by Johnson and German [21]. In the presence of a secondary phase such as Cu, densification evolves through three successive stages: (1) solid-state sintering before the melting of Cu; (2) W particle rearrangement driven by the formation of the liquid phase; (3) shrinkage of the W skeleton [5,16,17]. The objective of the present work is to confront experimental kinetics to computational predictions in view of assessing our understanding of the process of shrinkage of the solid skeleton during stage (3) with and without the presence of a liquid phase.

It is commonly agreed in literature that, in the temperature range usual for pressure-less sintering of crystalline materials, the

* Corresponding author.
E-mail addresses: francis.delannay@uclouvain.be (F. Delannay), Jean-Michel.Missiaen@phelma.grenoble-inp.fr (J.-M. Missiaen).

rate-limiting mechanism for densification is diffusion along grain boundaries rather than diffusion through grain bulk. In the presence of open porosity, grain growth is controlled by pore-drag, i.e. by transport inside the pores, from surface to surface. Owing to the very low partial pressure of W in the gas phase and to the very low solubility of W in liquid Cu, it is also commonly assumed that the rate-limiting mechanism for grain growth is diffusion along pore surface rather than transport across pore volume via evaporation/condensation or dissolution precipitation. This assumption will be assessed in the Appendix at the end of this paper. If densification and grain growth are governed by these two mechanisms, the difference of densification kinetics between systems W and W-Cu is expected to arise from only two factors: the difference of sintering stress arising from the filling of the pores by either only vapour or both liquid and vapour, and the difference of grain growth rate arising from the different diffusivity along W/Cu and W/vapour interfaces.

Densification kinetics is currently modelled using periodic 3D arrangements of identical particles in which grain coordination is constrained to keep integer values [1–12,21]. In the present work, densification kinetics is computed using a model able to account for arbitrary values of coordination. This model allows the capture of the change of sintering stress and sintering viscosity due to the increase in grain coordination with relative density. The simultaneous grain growth kinetics will be computed using the model of Riedel and Svoboda [1].

Section 2 presents the experimental observations that underlie the present work [20]. Comparison is made of two aggregates presenting the same volume fraction of W in the initial packing: an aggregate of pure W powder and a composite aggregate of W with 19 vol% of Cu. The focus is on the difference in the evolution of densification rate during isothermal holding at 1380 °C. Section 3 presents the model for the simulation of the sintering rate of the W skeleton with and without a liquid phase. For system W-Cu, a phenomenological law is proposed for representing the monotonically decreasing contribution of Cu/vapour interface to sintering stress during funicular filling of the pores by the liquid. Computational results are presented in Section 4. Good agreement with experimental observations is obtained when relying on admissible values of material parameters. The analysis suggests that diffusion along W/vapour interface is three times faster than along W/Cu interface. The sensitivity of model predictions to the uncertainties on the underlying hypotheses and on the values of material parameters is evaluated in Section 5.

2. Experimental methods and observations

This paper relies on the experimental work of Raharijaona et al. [20] who have investigated the difference in sintering kinetics between a compact of pure W powder and a compact prepared using the same W powder with addition of 10.0 wt% (= 19.3 vol%) of pure Cu powder. These two samples will be shortly designated “W” and “W-Cu”. Full details about experimental methods can be found in the original paper.

Fig. 1a presents a SEM micrograph of the pure W powder used for preparing both samples. Chemical analysis indicated the presence of only 85 ppm of C, 15 ppm of Co, and 14 ppm of Fe. The BET surface area was 1.7 $m^2\ g^{-1}$, which translates into an equivalent spherical grain diameter of 0.2 μm. For sample W-Cu, the powder mixture was obtained by milling the W powder with CuO powder of 1.8 μm equivalent BET diameter, followed by reduction at 623 K (350 °C) under He/H_2 flow. Cylinders of 8 mm diameter and 6 mm height were compacted uniaxially. The emphasis in the work of Raharijaona et al. [20] was to warrant the same skeleton density during the initial stage of the process. For this purpose, different compaction pressures were chosen for the two samples in such a way as to obtain the same initial fraction of 45 vol% of W in the compact. Accounting for the presence of Cu, this converts to a green density of 55% for sample W-Cu. The compacts were sintered under He/H_2 in a dilatometer allowing continuous monitoring of linear shrinkage. As shown on Fig. 2, the heat treatment involved successively.

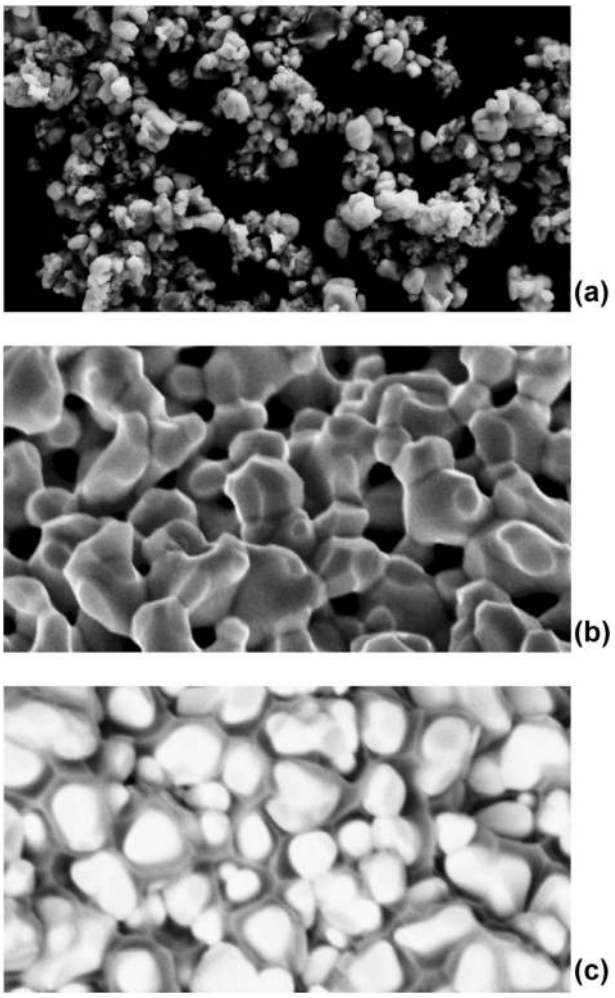

Fig. 1. SEM micrographs for comparison of W grain sizes (a) in the initial W powder, (b) in the pure W sample after sintering, and (c) in the W-19vol%Cu sample after sintering. b and c are reproduced from [20] by permission of Springer.

1. a heating ramp at 5 $Kmin^{-1}$ to 1050 °C,
2. a holding period of 1 h at 1050 °C to achieve full reduction of W,
3. a second ramp at 2.5 $Kmin^{-1}$ to 1380 °C,
4. a holding period of 120 min at 1380 °C
5. and a final cooling ramp at 20 $Kmin^{-1}$.

As illustrated on Fig. 1b and c, grain growth during the whole sintering process amounted to a similar factor in the two samples. According to measurements carried on SEM micrographs by computer-assisted image analysis, the mean linear intercept is 1.4 μm for W and 1.1 μm for W-Cu and the square root of the grain cross sectional area is 1.0 μm for W and 0.8 μm for W-Cu. These values should be taken with some caution as they are not obtained on true cross sections. Nevertheless, they indicate a lower grain growth in W-Cu, with a final size ratio $R_{GW\text{-}Cu}/R_{GW} \approx 0.8$ (we define R_G as the radius of a sphere of volume equal to the average grain

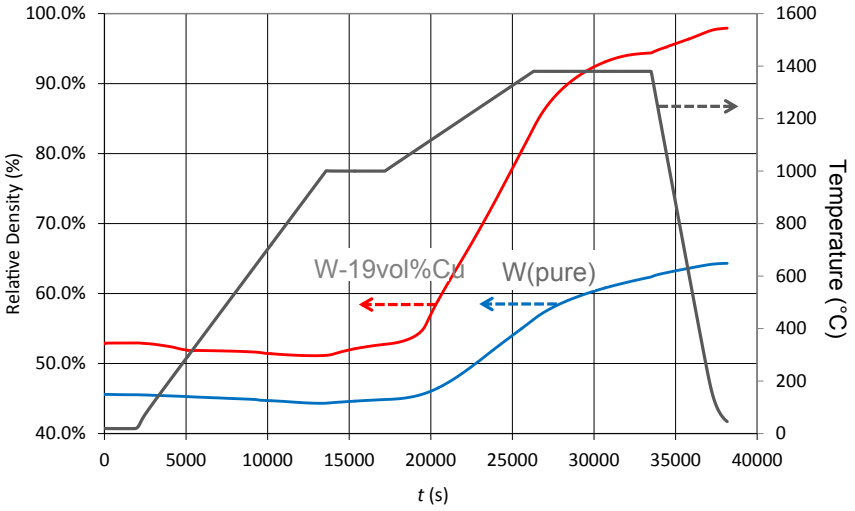

Fig. 2. Comparison of dilatometric curves during sintering of a pure W compact and a W-19vol%Cu compact (reproduced from [20] by permission of Springer). The two compacts had the same initial volume fraction of W before sintering.

volume).

In Ref. [20], two sintering phenomena were identified to occur before reaching the temperature of the plateau at 1380 °C:

1. In both samples, a slight densification by solid-state sintering was noticed to occur already during the reduction plateau at 1050 °C, i.e. before the melting of copper.
2. A strong enhancement of the densification rate of sample W-Cu was observed during the following heating ramp above the melting of Cu at 1083 °C. This phenomenon is not observed during sintering of sample W and can thus be identified as densification due to particle rearrangement driven by the capillary forces brought by the liquid phase. It peaks in the temperature interval between 1083 °C and 1200 °C and ends before the plateau temperature of 1380 °C is reached.

In order to leave aside the effects related to the temperature dependence of interface tensions and diffusivities, comparison of experimental observations with modelling predictions will be restricted to the portions of the curves of Fig. 2 recorded during the isothermal holding plateau of 120 min at 1380 °C. The rearrangement stage in W-Cu is thus not analysed. Measurements of the height and diameter of the cylinders after sintering revealed some shrinkage anisotropy. Care was taken to correct for this anisotropy when converting the dilatometry data into relative density curves. Fig. 3 shows the variation of the total densification rate, $d\rho_{total}/dt$, as a function of sample density, ρ_{total}, during the holding plateau at 1380 °C. Notice the difference of notation between ρ_{total} and the skeleton density ρ: $\rho = \rho_{total}$ in sample W whereas $\rho = 0.807\ \rho_{total}$ in sample W-Cu. Correspondingly to Fig. 3, the measured variation of $d\rho/dt$ with ρ is presented in Fig. 8a (dotted curves denoted "experimental"). In sample W, density increases from $\rho = 0.563$ to $\rho = 0.623$. In sample W-Cu, the total density increases from $\rho_{total} = 0.837$ to $\rho_{total} = 0.944$, which converts into a range of skeleton density $0.675 < \rho < 0.761$. In Refs. [18,22], similar densities and grain sizes were reported after isothermal sintering for 1 h at 1400 °C of W and W-10wt%Cu samples with initial W grain size of 0.23 μm. The larger skeleton density of sample W-Cu at the beginning of the plateau at 1380 °C results from the particle rearrangement stage as well as from the enhancement of densification rate during the heating ramp in the presence of liquid Cu (the latter effect will be discussed in Section 5).

In sample W, densification rate decreases along a curve that shows a continuous upward curvature whereas, in sample W-Cu, the curve shows an inflexion point at $\rho_{total} \approx 0.930$ (or $\rho \approx 0.750$), i.e. after 70 min of holding at 1380 °C. This inflexion point is followed by a drop to zero at $\rho_{total} \approx 0.945$ (or $\rho \approx 0.760$). In principle, provided the liquid phase does not exude from the specimen, full arrest of densification is expected when the vapour phase has been completely expelled from the porosity. The densification arrest at $\rho_{total} \approx 0.945$ can thus be interpreted as reflecting the fact that 5.5% of the volume consists of vapour phase that has been trapped inside the specimen. Indeed, as the liquid phase fills smaller pores before larger ones (this phenomenon is further discussed in Section 3),

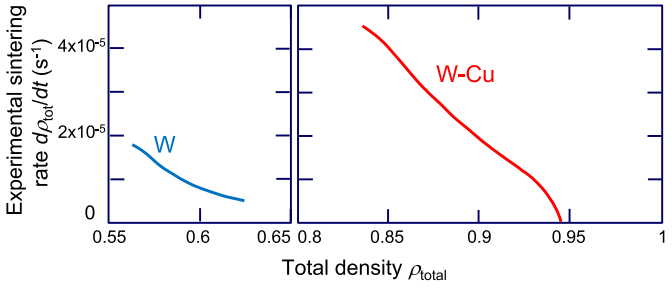

Fig. 3. Variation of the total densification rate $d\rho_{total}/dt$ as a function of the sample density during the two hours of holding at 1380 °C. The curves are derived from the dilatometric curves of Fig. 2.

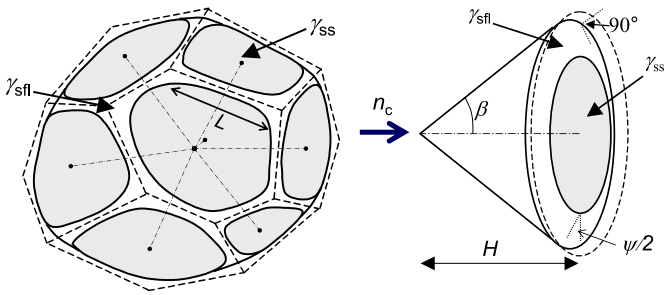

Fig. 4. The grains forming the aggregate are modelled as equivalent to n_c revolution cones of height H and half angle β at the apex (adapted from [25] and [38] by permission of Elsevier and Taylor & Francis).

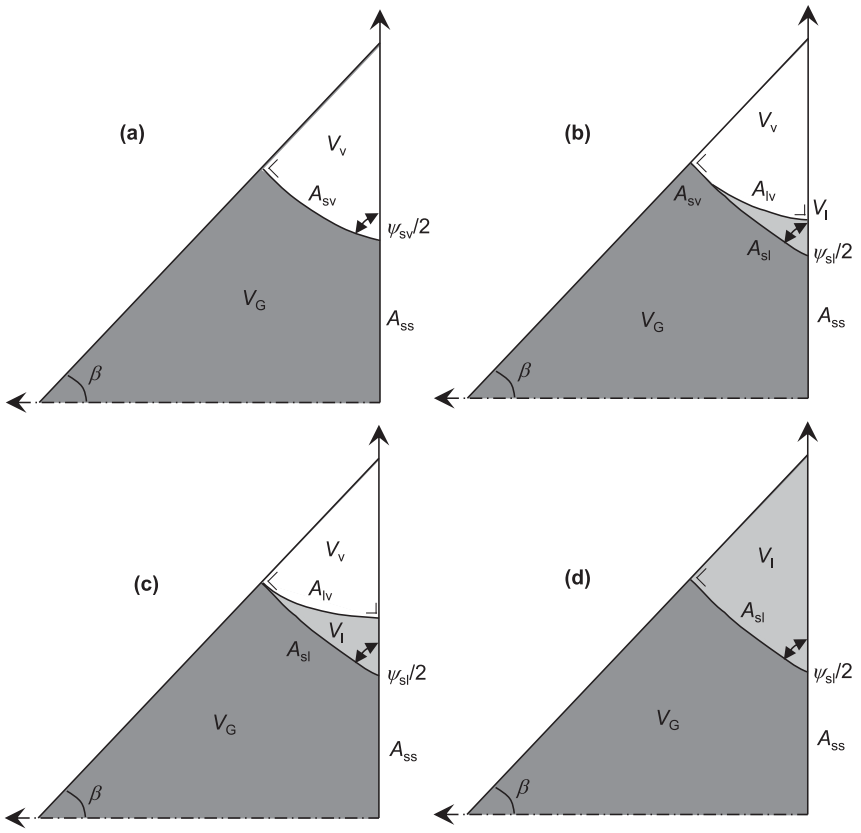

Fig. 5. The four cases to be distinguished: (a) Pores contain only vapour. (b) There exists a triple line solid/liquid/vapour delineating the liquid rings growing around grain boundaries. (c) The volume of the liquid rings is equal to the threshold for full coverage of the solid surface in the pores. (d) Pores contain only liquid. Cases (c) and (d) coexist during the funicular stage.

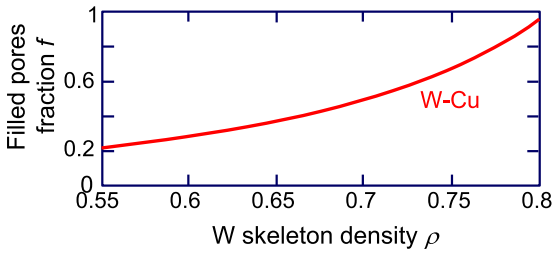

Fig. 6. Evolution, as a function of skeleton density, of the fraction f of pores filled with liquid in sample W-Cu during the funicular stage, assuming a constant grain size.

some amount of vapour phase can remain trapped in larger pores located remotely from the outer specimen surface. Consequently, the correspondence between experimental and predicted densification rates in sample W-Cu will be assessed only for the portion of the curve anterior to the inflexion point, i.e. for the first 70 min of holding at 1380 °C.

3. Modelling of densification kinetics

It is assumed that, when entering the isothermal holding plateau at 1380 °C, both systems present a fully continuous porosity with quasi uniform surface curvature. For solid state sintering, this situation is commonly designated as the intermediate stage of sintering. The presence of closed pores is thus not considered. Pores are filled either only by vapour, or only by liquid Cu, or simultaneously by liquid Cu and vapour. It is further assumed that, as well in pure W as in W-Cu, the rate-limiting transport mechanism that governs densification of the tungsten skeleton is diffusion of W along grain boundaries. In addition, for allowing the systems to be modelled as evolving under quasi-equilibrium, i.e. with interface curvatures taken as uniform, it is assumed that W transport from surface to surface inside the pores (either by surface diffusion or by diffusion across the phase occupying the pores) is much faster than W transport by diffusion along grain boundaries [4,11]. This assumption will be evaluated in Section 5.

Interfaces are considered energetically isotropic. Table 1 presents the values of interfacial tension at 1380 °C reported by Hodkin et al. [23] and Keene [24]. The corresponding dihedral angles are $\psi_{sv} = 2\arccos(\gamma_{ss}/2\gamma_{sv}) = 158°$ and $\psi_{sCu} = 2\arccos(\gamma_{ss}/2\gamma_{sCu}) = 116°$. The fact that $\gamma_{sv} > \gamma_{sCu} + \gamma_{Cuv}$, implies that $\theta = 0$, i.e. that solid W is perfectly wetted by liquid copper at 1380 °C.

3.1. Representative volume

The aggregate of W grains may be divided into Voronoï cells embedding each grain (Fig. 4). For deriving the representative volume element, the model considers an average cell consisting of a regular polyhedron of which

- the number of faces is equal to the average coordination number, n_c, of the grains
- and the volume is equal to $(4/3)\pi R_G^3/\rho$, where ρ is the relative density of the solid skeleton.

This cell is an assembly of n_c pyramidal prisms, of which the apex is the centre of gravity of the grain and the basis is one of the

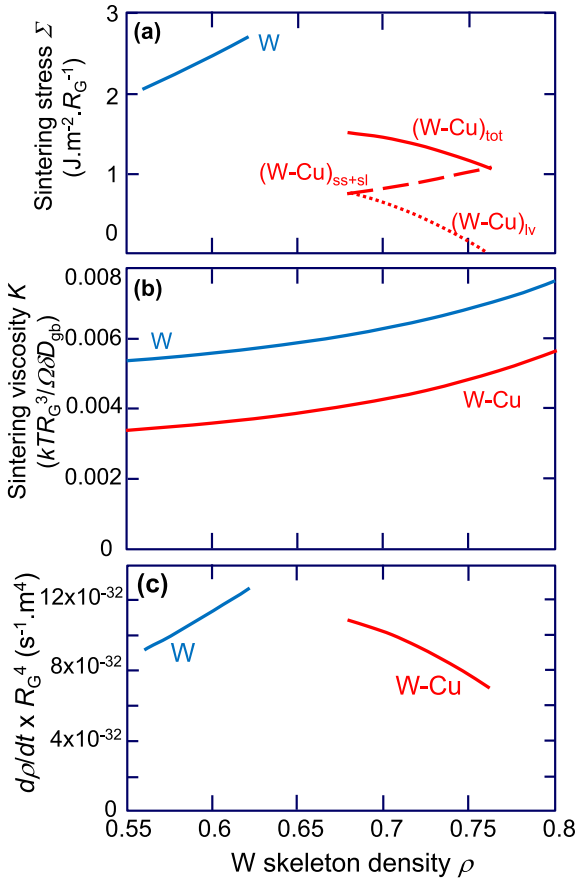

Fig. 7. Variation as a function W skeleton density ρ of (a) sintering stress Σ, (b) sintering viscosity K and (c) skeleton densification rate $d\rho/dt$ multiplied by the 4th power of the grain size R_G. For sample W-Cu, the total sintering stress $(W\text{-}Cu)_{tot}$ is the sum of a contribution denoted $(W\text{-}Cu)_{lv}$ (dotted line) due to the liquid/vapour interface and a contribution denoted $(W\text{-}Cu)_{sl}$ (dashed line) due to the combined effect of solid/liquid + solid/solid interfaces.

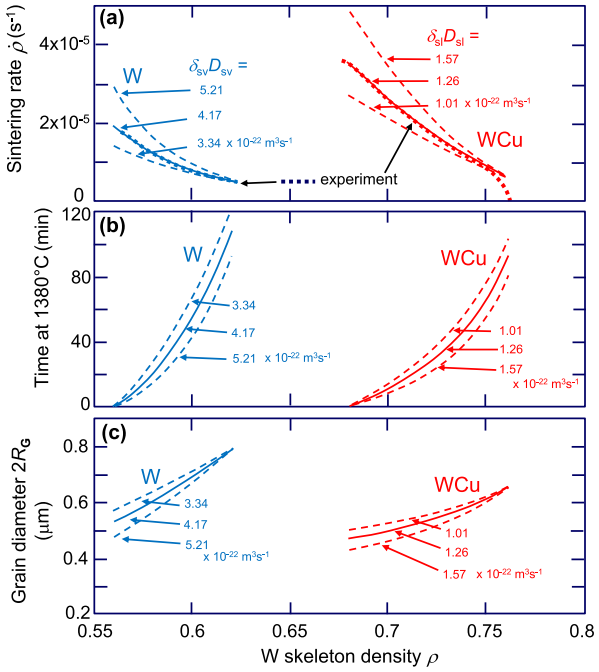

Fig. 8. Predicted variation, as a function of W skeleton density ρ, of (a) the sintering rate, $\dot{\rho}$, (b) the time at 1380 °C to reach density ρ, and the grain diameter, $2R_G$. The dashed lines are obtained when choosing $\delta_{sv}D_{sv}$ and $\delta_{sl}D_{sl}$ values departing by a factor of 1.25 from the optimum.

cell faces circumscribed by a ring of pore. As sketched in Fig. 4, these n_c pyramidal prisms can be approximated by n_c identical cones of revolution, of which the axis is the vector connecting the centres of gravity of the particles in contact and the height, H, is half the average distance between the centres of gravity. By symmetry, the solid/pore interface meets the external cone surface at 90°. The angle β at the cone apex is related to the average coordination number n_c as

$$\beta = \arccos\left(1 - \frac{2}{n_c}\right) \tag{1}$$

The model of Fig. 4 was initially developed for analysing capillary equilibrium in two phase systems consisting of aggregates of solid particles with a percolating liquid or vapour phase [25–28]. Under quasi-equilibrium, the interfaces solid/liquid, solid/vapour, and liquid/vapour that are enclosed within the representative cone are axisymmetric surfaces with uniform average curvature. The family of surfaces presenting this property is called Delaunay surfaces or nodoids, and the curves generating these surfaces are called Delaunay roulettes [29,30].

A particular feature of the representation of Fig. 4 is that computations can be carried out whatever the value of n_c, which does not need to be an integer. It is well documented that, during sintering of random aggregates, n_c increases monotonically with ρ. The initial coordination number can vary widely depending on the technique used for preparing the green part. The highest coordination in a random packing of identical spheres is about 6.2 [31]. At the other end, when ρ tends to 1, n_c reaches a maximum, which is equal to the average grain coordination in a dense, random polycrystal. There is a wide consensus that this maximum is in the range $13 < n_c < 14$ (e.g. Refs. [32,33]). Based on an extensive compilation of experimental data reported in literature, German [34] has shown that a good empirical fit of the evolution of coordination during densification is obtained using

$$n_c = 2 + 11\rho^2 \tag{2}$$

This law is used in all computations carried out in the present work.

In Fig. 5, the different cases to be potentially considered in systems W and W-Cu are illustrated by four cross-sections through the axis of the representative cone. V_G, V_l, and V_v denote the volumes of solid, liquid, and vapour in the cone. At any temperature, V_l/V_G is determined by the composition of the system.

- Fig. 5a: Porosity contains only vapour. The dihedral angle is $\psi_{sv} = 158°$.
- Fig. 5b: Grain boundaries are circumscribed by "pendular" liquid rings isolated from one another. The dihedral angle is $\psi_{sCu} = 116°$. The liquid/vapour interface meets the basis of the representative cone at 90°. There exists a triple line solid/liquid/vapour. As $\theta = 0$ in system W-Cu, pendular rings are interconnected via a thin liquid film covering the solid surface.
- Fig. 5c: The volume of pendular rings is equal to the threshold for disappearance of the triple line solid/liquid/vapour.
- Fig. 5d: Porosity is filled with liquid. There is no more liquid/vapour interface inside the porosity. Nevertheless, liquid/vapour interface exists at the external surface of the aggregate, forming menisci at the mouth of the pores. If densification of the solid

Table 1
Material parameters at 1380 °C for systems W and W-Cu.

γ_{sl}	1.02 J m^{-2}	[23]
γ_{ss}	1.08 J m^{-2}	[23]
γ_{sv}	2.83 J m^{-2}	[23]
γ_{lv}	1.15 J m^{-2}	[24]
D_{gb0}	1.1×10^{-3} m^2 s^{-1}	[21]
Q_{gb}	378 kJ mol^{-1}	[21]
δ_{gb}	0.5×10^{-9} m	[21]
$\delta_{gb}D_{gb}$	6.24×10^{-25} m^3 s^{-1}	
Ω_W	9.47×10^{-6} m^3 mol^{-1}	

skeleton further progresses, these menisci coalesce and the aggregate get immersed into an excess of liquid.

Let us consider an aggregate W-Cu starting in the pendular stage illustrated in Fig. 5b. After a certain decrease of V_v due to densification, the fraction $V_l/(V_G + V_l + V_v)$ in the porosity will become equal to the critical value corresponding to Fig. 5c: the system then enters the so-called "pore filling stage" or "funicular stage" [5,35,36]. As noticed by Svoboda et al. [5], during that stage, the system is subdivided in two parts corresponding to Fig. 5c and d: one part of pore channels is full of liquid (Fig. 5d) whereas the other part contains a meniscus of liquid of volume just equal to the threshold illustrated in Fig. 5c. Densification of the solid skeleton brings about the progressive increase of the part of the porosity network filled with liquid. The fraction of f of porosity filled by liquid is then a function of skeleton density and V_l/V_G ratio. The liquid being fully interconnected, the (concave) curvature of the liquid/vapour interface is the same everywhere, which means that the curvature of the menisci forming at the mouth of the pores is identical to the curvature of the menisci at the bottom of the pores containing vapour (Fig. 5c). Hence, during the funicular stage, the liquid/vapour curvature is determined by the size of the pores. It will be shown in Section 4 that sample W-Cu has entered the funicular stage of sintering well before the beginning of the isothermal holding at 1380 °C. Only the funicular stage will thus be considered in the following for system W-Cu.

Making use of a single average representative grain size R_G, the cone model predicts that, during the funicular stage, the curvature of the liquid/vapour meniscus increases with increasing solid skeleton density until it drops abruptly to zero when the last volume of vapor is expelled (i.e. at $\rho_{total} = 1$), before the liquid starts to be squeezed out of the aggregate. This is not realistic because the actual 3D shape of the porosity network and the inherent distribution of grain size implies a distribution of pore channel size [5,36,37]. During the funicular stage, the filling of the pores by the liquid progresses from the smaller pore channels to the larger ones, which brings the liquid/vapour interface curvature to decrease monotonically until it finally drops to zero at $\rho_{total} = 1$.

3.2. Densification rate

Pressure-less-sintering of a homogeneous, isotropic aggregate does not involve shear deformation. Using the convention of summation over repeated indices, the macroscopic densification rate $\dot{\rho}$ can then be expressed as [2,3,6,7]

$$\frac{\dot{\rho}}{\rho} = -\dot{\varepsilon}_{ii} = \frac{\Sigma}{K} \tag{3}$$

where Σ is the sintering stress and K is the bulk sintering viscosity.

The sintering stress Σ is the partial derivative of the Helmholtz free energy, F, with respect to the volume of porosity [2,6]:

$$\Sigma = \left(\frac{\partial F}{\partial(V_l + V_v)}\right)_{n_c, V_G} \tag{4}$$

In the presence of solid, liquid, and vapour, F writes

$$F = \gamma_{ss}A_{ss} + \gamma_{sl}A_{sl} + \gamma_{lv}A_{lv} + \gamma_{sv}A_{sv} \tag{5}$$

Using the cone model (Figs. 4 and 5), it is a matter of mathematics to derive the dependence of A_{sv}, A_{sl}, A_{ss} and A_{lv} on the parameters ρ, n_c, V_G, V_l and ψ. It has been shown that approximating by an arc of circle the curves generating the nodoids does not cause a large error in the computations [38]. Surface areas can then be expressed in the form of analytical expressions which can be retrieved in Refs. [25,38–40]. According to Eq. (5), Σ can, in general, be the sum of four contributions:

$$\Sigma = \Sigma_{ss} + \Sigma_{sl} + \Sigma_{lv} + \Sigma_{sv} \tag{6}$$

Only the first and last terms contribute in sample W whereas only the three first terms contribute in sample W-Cu during the funicular stage (because the pore surface is then covered by liquid).

Σ_{ss}, Σ_{sl} and Σ_{sv} scale as R_G^{-1} but Σ_{lv} does not because, as mentioned at the end of section 3.1, A_{lv} is not defined by the average grain size R_G because the size of the pore channels where the liquid/vapour menisci are located increases progressively. In order to bring about a flat meniscus surface in the framework of the cone model, the pore channel size must reach infinity at $\rho_{total} = 1$. When computing Σ_{lv}, this condition has been met by using an effective grain size R_{Geff} which increases with ρ up to ∞ at $\rho_{total} = 1$. A simple phenomenological law for this purpose is

$$R_{Geff} = \frac{\rho_f - \rho_{in}}{\rho_f - \rho} R_G \tag{7}$$

in which ρ_f is the skeleton density at $\rho_{total} = 1$. R_{Geff} must not be interpreted as a size belonging to the actual grain size distribution. Indeed, when ρ_{total} comes closer to 1, the large pore channels in which the liquid menisci are located are surrounded by a large number of grains. The pore channel size is thus not anymore defined by grain size according to the scheme of Figs. 4 and 5. The sole adjustable parameter in Eq. (7) is the density ρ_{in} at which $R_{Geff} = R_G$. As Σ_{lv} scales as γ_{lv}/R_{Geff}, Eq. (7) is equivalent to the use of an effective interface tension γ_{lveff} that decreases linearly in the interval $\rho_{in} \le \rho \le \rho_f$. Eq. (7) is simpler than the law proposed by Svoboda et al. [5] (Eq. (33) of the paper) which involves two or three adjustable parameters and does not bring about zero curvature at $\rho_{total} = 1$.

Following the method introduced by Riedel et al. [3], bulk viscosity, K, can be obtained in the framework of the cone model by equating the macroscopic dissipation rate to the dissipation rate resulting from the velocities and drag forces on the n_c cell faces. In the case of dissipation by grain boundary diffusion, one obtains [40].

$$K = \frac{1}{48}\left(\frac{(n_c - 2)^2}{n_c(n_c - 1)}\right)^{2/3} n_c \rho^{1/3} \left(\frac{c}{R_G}\right)^4 \frac{kTR_G^3}{\Omega \delta_{gb} D_{gb}} \tag{8}$$

where c is the radius of the grain boundary, Ω is the atomic volume, k is Boltzmann's constant, D_{gb} is the grain boundary diffusion coefficient of W and δ_{gb} the grain boundary diffusion thickness. At given ρ, K is different in samples W and W-Cu because c varies with ψ. The dependence of c on the parameters ρ, n_c, V_G, V_l and ψ can be calculated using the cone model. It has been shown that the values of Σ and K calculated in this way agree very well with the results of computations making use of regular packings of spheres [27,40].

It follows from Eqs. (3), (4), (7) and (8) that, for sintering

controlled by grain-boundary-diffusion, the densification rate $\dot{\rho}$ varies as R_G^{-4}. Proper modelling of the grain growth rate $\dot{R}_G$ during sintering is thus mandatory. As long as pores remain attached to grain boundaries, their presence profoundly affects grain growth during sintering. This phenomenon has been modelled by several authors [1,41,42]. We will rely on the model developed by Riedel and Svoboda [1] which assumes that the transport mechanism inside the pores is via surface diffusion. This assumption is evaluated in the Appendix. According to this model, during the regime of pore-drag control, the grain growth rate can be expressed as

$$\dot{R}_G = \frac{10p(\psi)\gamma_{ss}\Omega\delta_s D_s}{16kT}\frac{1}{R_G^3(1-\rho)^{3/2}} \quad (9)$$

where $p(\psi)$ is a dimensionless function of the dihedral angle ψ whereas D_s and δ_s are the diffusion coefficient and the diffusion thickness for W migration along the pore surface. A similar relationship, not including the role of dihedral angle, has been proposed by Du and Cocks [43]. Commonly, grain growth kinetics is represented by a power law $\dot{R}_G \propto R_G^{-m}$, i.e. $R_G^{m+1} - R_{G0}^{m+1} \propto t$. As densification progresses, R_G increases while $(1-\rho)$ decreases. Hence, it follows from Eq. (9) that $m < 3$.

4. Results

As shown in Section 2, isothermal sintering rates at 1380 °C were measured in the density ranges $0.56 \le \rho \le 0.62$ for sample W and $0.68 \le \rho \le 0.76$ for sample W-Cu. According to Eq. (2), n_c increases across these intervals from 5.45 to 6.23 in sample W and from 7.08 to 8.37 in sample W-Cu. Computational results presented in the following will either cover the whole range $0.55 \le \rho \le 0.80$ (Figs. 6 and 7b) or will be restricted to the density intervals pertinent for the two samples.

First, we have to identify the stage of sintering in sample W-Cu during isothermal holding. Computation according to the model shows that, at $\rho = 0.55$ (i.e. with $n_c = 5.3$), the threshold liquid fraction for full coverage of the solid surface by liquid (Fig. 5c) is $V_{Cu}/(V_{Cu} + V_W) = 0.073$, which is lower than the overall sample fraction $V_{Cu}/(V_{Cu} + V_W) = 0.193$. This means that part of the pores in sample W-Cu was already filled by liquid when $\rho = 0.55$, i.e. the funicular stage has been entered well before reaching the temperature of the isothermal sintering plateau. This is confirmed in Fig. 6 which shows the evolution with ρ of the fraction f of porosity filled by liquid during the funicular stage, calculated assuming a constant grain size: f increases from 0.22 at $\rho = 0.55$ to 0.94 at $\rho = 0.8$.

Table 1 presents the nominal values of material parameters at 1380 °C that have been used for computing sintering stress and sintering viscosity. The value of $\delta_{gb}D_{gb}$ for W at 1380 °C is obtained via the Arrhenius law $D_{gb} = D_0 \exp(-Q_{gb}/kT)$ using the values of D_0, Q_{gb}, and δ_{gb} reported in Ref [21], which yields $\delta_{gb}D_{gb} = 6.24 \times 10^{-25}$ m^3 s^{-1}. No data is given in Table 1 for the surface diffusion coefficient $\delta_{Wv}D_{Wv}$ and $\delta_{WCu}D_{WCu}$ because these parameters will be deduced by fitting experimental curves with model predictions. The values inferred via the fitting procedure will be appraised in Section 5.

Fig. 7a shows the evolution of sintering stress, Σ, at given grain size. For sample W, the increase of Σ with ρ reflects the increase in solid/vapour surface curvature when pore size decreases. For sample W-Cu, different curves are drawn for different contributions to the sintering stress. The continuous curve, denoted (W-Cu)$_{total}$, is Σ total. The dashed curve, denoted (W-Cu)$_{ss+sl}$, is the sum of contributions $\Sigma_{ss} + \Sigma_{sl}$ (Eq. (6)). This contribution increases with ρ similarly as Σ for sample W, but its magnitude is lower owing to two differences: $\gamma_{sl} < \gamma_{sv}$; $\psi_{sl} < \psi_{sv}$. The dotted curve, denoted (W-Cu)$_{lv}$, is contribution Σ_{lv} computed using, in Eq. (7), $\rho_f = 0.76$ (i.e., according to Fig. 3, the skeleton density ρ at which densification is zero) and $\rho_{in} = 0.55$. The choice for ρ_{in} was made empirically to provide the best agreement with experimental kinetics (the sensitivity of computational results to the value chosen for ρ_{in} will be analysed in Section 5). The decrease of Σ_{lv} to zero at $\rho_{total} = 1$ is not linear because the increase of ρ and the increase of R_{Geff} have opposite effects on liquid/vapour surface curvature. One notices that, during most of the isothermal period, Σ_{lv} is smaller than $\Sigma_{ss} + \Sigma_{sl}$. The reverse is more common in liquid phase sintering because dihedral angle ψ_{sl} is commonly much smaller than 116°.

Fig. 7b shows the evolution of the sintering viscosity, K, calculated in the range $0.55 \le \rho \le 0.80$ for the two samples. The units for K being identical for the two samples, they have been left in $kTR_G^3/\Omega\delta_{gb}D_{gb}$. At the same ρ, K is lower in sample W-Cu because the lower dihedral angle brings about a lower grain boundary radius c in Eq. (8). The increase of K with ρ is due to the increase of c with ρ.

Fig. 7c shows the evolution of the product $\dot{\rho}\,R_G^4$ at given grain size. For sample W, $\dot{\rho}\,R_G^4$ increases with ρ because Σ increases with ρ more than K. For sample W-Cu, $\dot{\rho}\,R_G^4$ decreases with increasing ρ, which is primarily due to the decrease of Σ_{lv} with ρ.

In Fig. 8, the curves $\dot{\rho}\,R_G^4$ of Fig. 7c have been combined with the grain growth law (Eq. (9)) to derive the evolution of the skeleton densification rate $\dot{\rho}$ (Fig. 8a), of the time of holding at 1380 °C needed to reach density ρ (Fig. 8b), and of the grain diameter $2R_G$ (Fig. 8c). In Eq. (9), $p(\psi)$ was calculated using the law proposed in Ref. [1] whereas the values of $\delta_{sv}D_{sv}$ and $\delta_{sl}D_{sl}$ were inferred via a two-step procedure:

1. The value of $2R_G$ close to the end of the plateau, i.e. at $\rho = 0.62$ for sample W and $\rho = 0.75$ for sample W-Cu, is derived from the value of $\dot{\rho}\,R_G^4$ (Fig. 7c). The result is $2R_G = 0.79$ μm for sample W and $2R_G = 0.66$ μm for sample W-Cu (confer end points of the curves in Fig. 8c). It is worthwhile that these grain sizes, which are obtained by using solely the nominal parameters listed in Table 1, differ only by a factor 0.6–0.8 from the size parameters measured by image analysis (1.0–1.4 μm for W, 0.8–1.1 μm for W-Cu). In particular, the agreement with respect to the experimental ratio $R_{GW\text{-}Cu}/R_{GW} \approx 0.8$ is striking.
2. From these $2R_G$ values at $\rho = 0.62$ or $\rho = 0.75$, the evolution of $2R_G$ was computed via Eq. (9) by choosing the values for $\delta_{sv}D_{sv}$ and $\delta_{sl}D_{sl}$ that provide, for densification rates $\dot{\rho}$, minimum departure between experimental curves (dotted curves in Fig. 8a) and computed curves. The full curves in Fig. 8a–c are the results of this optimisation procedure: they were obtained using $\delta_{sv}D_{sv} = 4.17 \times 10^{-22}$ m^3.s^{-1} for sample W and $\delta_{sl}D_{sl} = 1.26 \times 10^{-22}$ m^3.s^{-1} for sample W-Cu. The standard deviation on the ratio $\frac{(\dot{\rho})_{exper}}{(\dot{\rho})_{model}}$ of experimental and computed curves is, respectively, 1.2% over the range $0.56 \le \rho \le 0.62$, and 0.9% over the range $0.68 \le \rho \le 0.75$. The excellence of the agreement for $\dot{\rho}$ across the whole density domain is thus quite conspicuous.

According to the full curves in Fig. 8c, W grain diameter $2R_G$ has, during the holding period at 1380 °C, increased from 0.47 μm to 0.66 μm in sample W and from 0.53 μm to 0.79 μm in sample W-Cu. Hence, grain sizes have increased from 0.2 μm to about 0.5 μm during the heating ramp to 1380 °C.

In order to assess the power law $\dot{R}_G \propto R_G^{-m}$ commonly used for grain growth, Fig. 9 presents, on a log–log scale, the variation of $\dot{R}_G$ as a function of R_G derived using the same optimised values for $\delta_{sv}D_{sv}$ and $\delta_{sl}D_{sl}$. For sample W, the power law appears well obeyed over the whole range, with an exponent m = 2.5. For sample W-Cu,

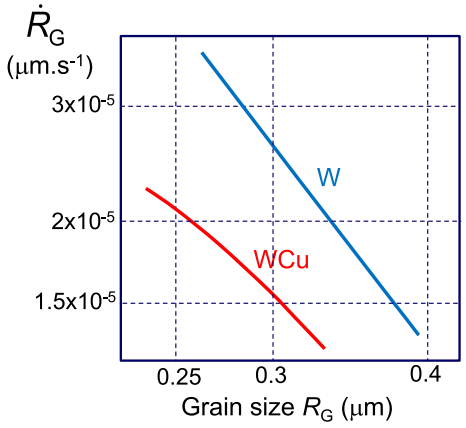

Fig. 9. Variation of the grain growth rate $\dot{R}_G$ as a function of the grain size R_G (log–log scale) calculated using $\delta_{sv}D_{sv} = 4.17 \times 10^{-22}$ m^3 s^{-1} for sample W and $\delta_{sl}D_{sl} = 1.26 \times 10^{-22}$ m^3 s^{-1} for sample W-Cu.

m increases when R_G increases, with an average m = 1.7. Hence, according to Eq. (9), R_G varies as $(1-\rho)^{-3}$ in sample W and more or less as $(1-\rho)^{-1.15}$ in sample W-Cu.

5. Discussion

The surface diffusivities $\delta_{Wv}D_{Wv} = 4.17 \times 10^{-22}$ m^3 s^{-1} and $\delta_{WCu}D_{WCu} = 1.26 \times 10^{-22}$ m^3 s^{-1} which were inferred via the optimisation procedure agree quite well with the diffusivity $\delta_{Wv}D_{Wv} = 1.43 \times 10^{-22}$ m^3 s^{-1} that can be calculated using the data proposed in Ref. [21] with an activation energy Q = 293 kJ mol^{-1}. These diffusivities are, respectively, 700 and 200 times larger than grain boundary diffusivity of W: $\delta_{gb}D_{gb} = 6.24 \times 10^{-25}$ m^3 s^{-1} (Table 1). A similar ratio $\delta_{sv}D_{sv}/\delta_{gb}D_{gb}$ has been identified between 1000 °C and 1100 °C for undoped zirconia and 3Y-TZP by Kanters et al. [14] (these authors follow a modelling and fitting procedure resembling that used in the present work). Such a large diffusivity ratio supports the initial hypothesis that the systems may be modelled as evolving under quasi-equilibrium.

The extraction of values for $\delta_{Wv}D_{Wv}$ and $\delta_{WCu}D_{WCu}$ from a comparison of model and experiment is based on the assumption (underlying the grain growth model [1]) that transport inside the pores occurs only via surface diffusion. The question arises of whether these surface diffusivity values are compatible with the assumption of dominance of surface transport with respect to transport by evaporation-condensation in the gas phase or dissolution-precipitation in liquid Cu. This issue is addressed in the Appendix. It is shown that, in sample W, transport via evaporation/condensation may indeed be neglected but that, in sample W-Cu, both surface transport and dissolution/precipitation may contribute to W transport inside the pores. Nevertheless, the results presented in Section 4 remain valid even if $\delta_{WCu}D_{WCu}$ involves a contribution of transport by dissolution/precipitation.

Whatever the transport mechanism, the results indicate that W transport inside the pores is three times slower in sample W-Cu than in sample W, in which transport occurs by diffusion at interface W/vapour. We believe that this difference is not fortuitous as it is well known that the surface diffusivity of W can be increased by the addition small amounts of "activator" such as Pd, Ni, Co, Fe, or Pt, which create a fast diffusion layer on the surface of tungsten [21]. This means that, in sample W, surface diffusivity might be enhanced by surface enrichment by trace elements present in the starting powder. In this case, the lower apparent diffusivity in system W-Cu could result from the dissolution of these trace elements into liquid copper. An possible alternative cause to be invoked is that chemical bonding with Cu would bring about an increase in the activation energy for surface diffusion of W.

The model involves 7 independent material parameters: $\delta_{gb}D_{gb}$, $\delta_{sv}D_{sv}$, $\delta_{sl}D_{sl}$, γ_{ss}, γ_{sv}/γ_{ss} (or ψ_{sv}), γ_{sl}/γ_{ss} (or ψ_{sl}), and γ_{lv}/γ_{ss}. The accuracy of simulations depends on the precision on these parameters. It is instructive to evaluate the sensitivity of the computational results to a change of each parameter individually.

- $\delta_{gb}D_{gb}$

The uncertainty on literature data for the value of $\delta_{gb}D_{gb}$ to be used at given temperature is quite large. The product $\dot{\rho}\,R_G^4$ scales as $\delta_{gb}D_{gb}$. This means that if the actual value of $\delta_{gb}D_{gb}$ was 2 times larger than the nominal value given in Table 1, the grain diameter curves in Fig. 8c would be shifted up by 19%, which would be more than sufficient to completely reconcile predicted grain sizes with experimental results.

- $\delta_{sv}D_{sv}$ and $\delta_{sl}D_{sl}$

The uncertainty on the actual value of $\delta_{sv}D_{sv}$ and $\delta_{sl}D_{sl}$ is also quite large The dashed curves on Fig. 8 show the effect of a departure by a factor of merely 1.25 from the values of $\delta_{sv}D_{sv}$ or $\delta_{sl}D_{sl}$ that were found to best fit the experimental curves for $\dot{\rho}$. The predicted grain growth rate at 1380 °C is changed by about 25% (Fig. 8c), which brings about a change by about 10% on the prediction of the holding time to obtain the same increase in density (Fig. 8b). The uncertainty on $\delta_{sv}D_{sv}$ and $\delta_{sl}D_{sl}$ has thus a larger influence on the simulations than the uncertainty on $\delta_{gb}D_{gb}$.

- γ_{ss}

γ_{ss} has the same effect as $\delta_{sv}D_{sv}$ and $\delta_{sl}D_{sl}$ on the grain growth rate (Eq. (9)) and the same effect as $\delta_{gb}D_{gb}$ on the product $\dot{\rho}\,R_G^4$. A multiplication or a division of the four interface tensions by the same correction factor (in such a way as to keep γ_{sv}/γ_{ss}, γ_{sl}/γ_{ss}, and γ_{lv}/γ_{ss} constant) would thus have a similar effect as the application of this correction factor on $\delta_{gb}D_{gb}$, $\delta_{sv}D_{sv}$ and $\delta_{sl}D_{sl}$. However, the uncertainty on the actual value of interface tensions is much lower that the uncertainty on diffusivities.

- γ_{sv} and γ_{sl} (i.e. ψ_{sv} and ψ_{sl})

The uncertainty on dihedral angle values is not expected to be very large. Fig. 10a shows the effect on $\dot{\rho}\,R_G^4$ of a correction by ± 30% on γ_{sv} or γ_{sl}. For γ_{sv}, the ensuing change of dihedral angle brings about a shift of the curve $\dot{\rho}\,R_G^4$ by about the same factor without change of the overall shape of the curve. This shift would mean a change of the predicted W grain size by merely ±7%. In contrast, applying the same correction factor to γ_{sl} has less effect on the absolute value of $\dot{\rho}\,R_G^4$ but it causes a change of the slope of the curve, which, as shown hereafter, implies different shapes of the grain growth kinetics curves.

- γ_{lv}

The dashed curves in Fig. 10b show the effect on $\dot{\rho}\,R_G^4$ of a multiplication or division of the nominal value of γ_{lv} by a factor 1.30. This change is exactly equivalent to a division or multiplication by the same factor of the difference $(\rho_f - \rho_{in})$ (Eq. (7)), i.e. it is equivalent to the choice $\rho_{in} = 0.49$ or $\rho_{in} = 0.60$ instead of $\rho_{in} = 0.55$. This change quite significantly modifies the slope of the decrease of $\dot{\rho}\,R_G^4$ with increasing ρ for sample W-Cu (Fig. 10b). Using the dashed curves of Fig. 10b, a change of $\delta_{sl}D_{sl}$ by ± 5% is required for best

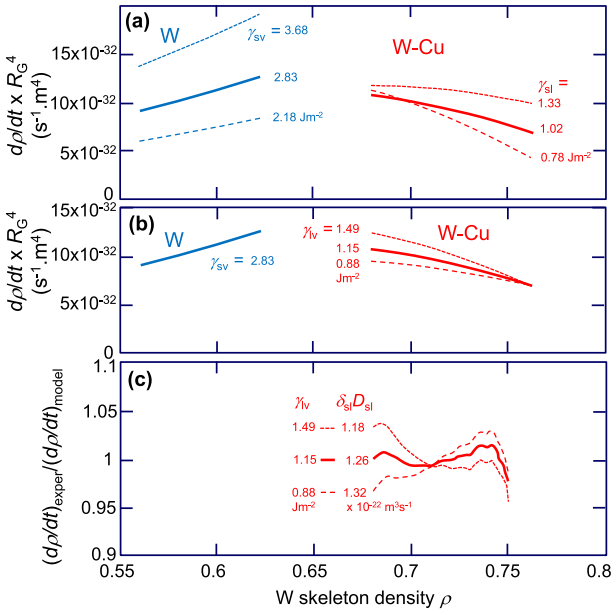

Fig. 10. (a) Effect of a 30% departure from the nominal value of γ_{sv} (for sample W) or γ_{sl} (for sample W-Cu) on the variation of the product $\dot{\rho}R_G^4$ as a function of W skeleton density. (b) Effect of a 30% departure from the nominal value of γ_{lv} in sample W-Cu. (c) For the same γ_{lv} values as in (b), variation of the ratio $\frac{(\dot{\rho})_{experiment}}{(\dot{\rho})_{model}}$ after adjustment of $\delta_{sl}D_{sl}$ for best correspondence between experimental and modelled curves.

fitting of experimental densification rates $\dot{\rho}$. The curves of Fig. 10c show that the quality of the fit, represented by the evolution of the ratio $\frac{(\dot{\rho})_{exper}}{(\dot{\rho})_{model}}$, is lowered: the standard deviation on $\frac{(\dot{\rho})_{exper}}{(\dot{\rho})_{model}}$ is doubled, from 0.9% for γ_{lv} = 1.15 J m^{-2} to 1.8% for γ_{lv} = 1.49 J m^{-2} or 0.88 J m^{-2}.

An extrapolation down to $\rho < 0.6$ of the curves $\dot{\rho}\, R_G^4$ for W-Cu in Fig. 10c suggests that, below $\rho = 0.6$, the densification rate is probably higher for W-Cu than for W. This means that the higher skeleton density in sample W-Cu at the end of the heating ramp to 1380 °C might be ascribed both to the densification brought about by the rearrangement stage at melting of Cu and to a higher densification rate at low ρ in sample W-Cu owing to the lower value of K and to the enhancement of Σ by the liquid/vapor contribution Σ_{lv}.

A final point of discussion is whether accounting in the computations for the increase of n_c with ρ (via Eq. (4)) makes a significant difference with respect to computations using a constant coordination n_c. The answer is yes. As detailed in Ref [44], an increase of n_c at given ρ brings about an increase of $\dot{\rho}$. It follows that computations using constant n_c significantly alter the shape of $\dot{\rho}\, R_G^4$ curves, which was found to reduce significantly the quality of the correspondence between $(\dot{\rho})_{exper}$ and $(\dot{\rho})_{model}$. For example, using constant $n_c = 8$ for W-Cu, the lowest standard deviation on $\frac{(\dot{\rho})_{exper}}{(\dot{\rho})_{model}}$ that could be achieved over the range $0.68 \leq \rho \leq 0.75$ (via the fitting procedure described above) was 5.0%, i.e. a fivefold increase with respect to the computations accounting for the increase of n_c with ρ.

6. Conclusion

The contributions of the paper can be summarized as follows.

- A model is presented for the simulation of the intermediate stage of sintering both in the absence and in the presence of a liquid phase. Mass transport is assumed to remain governed by grain boundary diffusion, i.e. negligible diffusion is assumed through the liquid phase. The model allows accounting for the monotonic increase in grain coordination with density. During funicular filling of the pores by the liquid, the contribution of liquid/vapour surface curvature to sintering stress is taken to decrease progressively owing to the progressive increase in the size of the pore channels remaining to be filled by liquid. A phenomenological law is proposed for this purpose. The effect of grain growth is simulated via the equation proposed by Riedel et al. [1].
- The model has been assessed by confronting its predictions to the experimental measurements of Raharijaona et al. [20] for the isothermal sintering at 1380 °C of pure W and of a composite of W-Cu with 19.3 vol% Cu.
- The presence of liquid Cu affects sintering stress in three ways: whereas a positive contribution is brought about by the concave curvature of the liquid/vapour surface in pores that are not yet filled with liquid, a reduction of sintering stress is caused by the fact that $\gamma_{W/Cu} < \gamma_{W/vapour}$, as well as by the ensuing decrease in dihedral angle. Conversely, the decrease in dihedral angle causes a decrease in bulk viscosity.
- Using a set of material parameter reported in literature, a good agreement is found between observed and predicted grain sizes at the end of sintering.
- For the evolution of densification rate with density, conspicuous agreement between experimental curves and model predictions is obtained by tuning the values of solid/vacuum and solid/liquid surface diffusivities. The diffusivity values optimized in this way appear consistent with values reported in literature.
- The analysis shows that model predictions are more sensitively affected by uncertainties on interface diffusivities than by uncertainties on interface tensions. Precision of interface diffusivity particularly affects the prediction for grain size. Accounting for the increase of n_c with ρ significantly improves the agreement with experiment.
- The work stresses the key role played by grain growth. Clearly, further validation of the model necessitates more detailed experimental data on sintering trajectories, i.e. on the kinetics of grain growth during sintering.

Acknowledgements

The experimental part of this work was carried out with the support of the EFDA (European Fusion Development Agreement) and the European Union under the contract of Association between EURATOM/CEA N° EUR 344-88 A FUA F. The authors also thank the company Eurotungstene Metal Powders for material supply and technical support. They gratefully acknowledge the help of Matthieu Marteleur for grain size measurements.

Appendix. Diffusion across pore volume or along pore surface

The flux of W arriving at – or exiting from – the pore surface via diffusion across the bulk of the pore writes

$$j = -\frac{D_b x_b}{V_{mb}} \frac{1}{RT} \nabla\mu \left(m^{-2}s^{-1}\right) \qquad \text{(A1)}$$

where $\nabla\mu$ is the gradient of chemical potential, V_{mb} the molar volume of the phase occupying the pore, and D_b and x_b are, respectively, the diffusion coefficient and the molar fraction of W in the bulk of that phase. The flux of W migrating along the pore surface via surface diffusion writes

$$j_s = -\frac{\delta_s D_s}{V_{mW}} \frac{1}{RT} \nabla\mu \left(m^{-1} s^{-1} \right) \quad \text{(A2)}$$

where V_{mW} is the molar volume of W. Denoting Ω the atomic volume of W, the normal velocity v_n of the grain surface due to the addition or withdrawal of W is, in the case of bulk diffusion, $v_n = \Omega j$, and in the case of surface diffusion, $v_n = -\Omega \nabla_s \cdot j_s$ where $\nabla_s \cdot$ is the divergence operator. The divergence of j_s can be approximated as $\approx j_s/\Delta z$ where Δz is a characteristic length of W diffusion. Δz being close to the grain size R_G, the relative importance of the mechanisms can be appreciated by comparing $D_b x_b/V_{mb}$ and $\delta_s D_s/(V_{mW} R_G)$ at 1653 K.

The vapour pressure of W can be expressed as $p_{vap}/p^\circ = \exp(-10^5 K/T + 18)$ [45], which yields $x_b = 3 \times 10^{-20}$. Cussler [46] reports the diffusion coefficient in H_2/H at 1 atm to be 10^{-4} $(T/300K)^{1/2}$ m^2 s^{-1}, which yields $D_b = 2 \times 10^{-4}$ m^2 s^{-1} (the influence of the mass and diameter of W on its diffusivity in the gas phase may be neglected for the present purpose [46]). The molar volume of H_2/H at 1 atm. is 22.4×10^{-3} (T/300K) $m^3 = 0.12$ m^3. Hence, $D_b x_b/V_{mb} \approx 5 \times 10^{-23}$ m^{-1} s^{-1}. In comparison, using $V_{mW} = 9.5 \times 10^{-6}$ m^3 with $\delta_{sv} D_{sv} = 4 \times 10^{-22}$ m^3 s^{-1} and $R_G \approx 0.3$ 10^{-6} m (Fig. 8) yields $\delta_{sv} D_{sv}/(V_{mW} R_G) \approx 1.3 \times 10^{-10}$ m^{-1} s^{-1}. The contribution of transport by evaporation/condensation is thus more than 12 orders of magnitude lower than the contribution due to surface diffusion.

The solubility of W in liquid Cu is very low: according to Eremenko et al. [47], $1.3 \times 10^{-7} > x_b > 0.3 \times 10^{-7}$ at 1673 K. For the diffusion coefficient of W in liquid Cu, we may take in the work of Szpunar and Smith [48] the value at 1650 K for a dilute solution of Au in Cu: $D_b = 5 \times 10^{-9}$ m^2 s^{-1}. The molar volume of Cu is $V_{mCu} = 7.1 \times 10^{-6}$ m^3. Hence, 9×10^{-11} m^{-1} $s^{-1} > D_b x_b/V_{mb} > 2 \times 10^{-11}$ m^{-1} s^{-1}. In comparison, using $\delta_{sv} D_{sv} = 1 \times 10^{-22}$ m^3 s^{-1} and $R_G \approx 0.25$ 10^{-6} m (Fig. 8) yields $\delta_{sv} D_{sv}/(V_{mW} R_G) \approx 4 \times 10^{-11}$ m^{-1} s^{-1}. It thus appears that, in system W-Cu, surface diffusion and dissolution/precipitation may both contribute to W transport inside the pores.

References

[1] H. Riedel, J. Svoboda, A theoretical study of grain growth in porous solids during sintering, Acta Metall. Mater. 41 (1993) 1929–1936.
[2] J. Svoboda, H. Riedel, H. Zipse, Equilibrium pore surfaces, sintering stresses and constitutive equations for the intermediate and late stages of sintering- I computation of equilibrium surfaces, Acta Metall. Mater. 42 (1994) 435–443.
[3] H. Riedel, H. Zipse, J. Svoboda, Equilibrium pore surfaces, sintering stresses and constitutive equations for the intermediate and late stages of sintering—II. Diffusional densification and creep, Acta Metall. Mater. 42 (1994) 445–452.
[4] J. Svoboda, H. Riedel, Quasi-equilibrium sintering for coupled grain-boundary and surface diffusion, Acta Metall. Mater. 43 (1995) 499–506.
[5] J. Svoboda, H. Riedel, R. Gaebel, A model for liquid phase sintering, Acta Mater. 44 (1996) 3215–3226.
[6] F. Wakai, Y. Shinoda, T. Akatsu, Methods to calculate sintering stress of porous materials in equilibrium, Acta Mater. 52 (2004) 5621–5631.
[7] F. Wakai, T. Akatsu, Y. Shinoda, Shrinkage and disappearance of a closed pore in the sintering of particle cluster, Acta Mater. 54 (2006) 793–805.
[8] F. Wakai, Y. Shinoda, Anisotropic sintering stress for sintering of particles arranged in orthotropic symmetry, Acta Mater. 57 (2009) 3955–3964.
[9] F. Wakai, Comment on "Local vs. global approach in the analysis of sintering kinetics", Scr. Mater. 62 (2010) 117–119.
[10] F. Wakai, T. Akatsu, Anisotropic viscosities and shrinkage rates in sintering of particles arranged in a simple orthorhombic structure, Acta Mater. 58 (2010) 1921–1929.
[11] F. Wakai, K.A. Brakke, Mechanics of sintering for coupled grain boundary and surface diffusion, Acta Mater. 59 (2011) 5379–5387.
[12] F. Wakai, R.K. Bordia, J. Blendell, Microstructural evolution and anisotropic shrinkage in constrained sintering and sinter forging, J. Am. Ceram. Soc. 95 (2012) 2389–2397.
[13] T. Kraft, H. Riedel, Numerical simulation of solid state sintering; model and application, J. Eur. Ceram. Soc. 24 (2004) 345–361.
[14] J. Kanters, U. Eisele, H. Böder, J. Rödel, Continuum mechanical description of sintering nanocrystalline zirconia, Adv. Eng. Mater. 3 (2001) 158–162.
[15] C.H. Allibert, S. Lay, F. Dore, Densification of W-Cu powder with submicron size microstructure, Mater. Sci. Forum 426 (2003) 4197–4202. Trans Tech Publ.
[16] F. Doré, C.L. Martin, C.H. Allibert, Apparent viscosity of W–Cu powder compacts during sintering, Mater. Sci. Eng. A 383 (2004) 390–398.
[17] J.L. Johnson, J.J. Brezovsky, R.M. German, Effect of liquid content on distortion and rearrangement densification of liquid-phase-sintered W-Cu, Metal. Mater. Trans. A 36 (2005) 1557–1565.
[18] J.L. Johnson, J.J. Brezovsky, R.M. German, Effects of tungsten particle size and copper content on densification of liquid-phase-sintered W-Cu, Metal. Mater. Trans. A 36 (2005) 2807–2814.
[19] J. Raharijaona, J. Missiaen, R. Mitteau, Coupling between sintering and liquid migration to process tungsten-copper functionally graded materials, Adv. Sinter. Sci. Technol. Ceram. Trans. 87 (2010) 321–333.
[20] J.-J. Raharijaona, J.-M. Missiaen, D. Bouvard, A phenomenological analysis of sintering mechanisms of W-Cu from the effect of copper content on densification kinetics, Metal. Mater. Trans. A 42 (2011) 2411–2419.
[21] J.L. Johnson, R.M. German, Theoretical modeling of densification during activated solid-state sintering, Metal. Mater. Trans. A 27 (1996) 441–450.
[22] J.L. Johnson, Activated liquid phase sintering of W–Cu and Mo–Cu, Int. J. Refract. Metals Hard Mater. (2015). http://dx.doi.org/10.1016/j.ijrmhm.2015.04.030.
[23] E. Hodkin, M. Nicholas, D. Poole, The surface energies of solid molybdenum, niobium, tantalum and tungsten, J. Less Common Metals 20 (1970) 93–103.
[24] B. Keene, Review of data for the surface tension of pure metals, Int. Mater. Rev. 38 (1993) 157–192.
[25] F. Delannay, D. Pardoen, C. Colin, Equilibrium distribution of liquid during liquid phase sintering of composition gradient materials, Acta Mater. 53 (2005) 1655–1664.
[26] C. Colin, V. Guipont, F. Delannay, Equilibrium distribution of liquid during sintering of assemblies of WC/Co cermets, Metal. Mater. Trans. A 38 (2007) 150–158.
[27] F. Delannay, J.M. Missiaen, Experimental validation of a new model for the initial stage of sintering of single phase systems, Acta Mater. 57 (2009) 420–431.
[28] N. Limodin, L. Salvo, M. Suéry, F. Delannay, Capillary equilibrum in semi-solid Al-Cu slurry, Int. J. Mater. Res. 101 (2010) 265–270.
[29] C. Delaunay, Sur la surface de révolution dont la courbure moyenne est constante, J. Math. pures appliquees (1841) 309–314.
[30] W. Carter, The forces and behavior of fluids constrained by solids, Acta Metall. 36 (1988) 2283–2292.
[31] G.D. Scott, Radial distribution of the random close packing of equal spheres, Nature 194 (1962) 956–957.
[32] E. Arzt, The influence of an increasing particle coordination on the densification of spherical powders, Acta Metall. 30 (1982) 1883–1890.
[33] M.E. Glicksman, Analysis of 3-D network structures, Philos. Mag. 85 (2005) 3–31.
[34] R.M. German, Coordination number changes during powder densification, Powder Technol. 253 (2014) 368–376.
[35] K. Lappalainen, M. Manninen, V. Alopaeus, J. Aittamaa, J. Dodds, An analytical model for capillary pressure–saturation relation for gas–liquid system in a packed-bed of spherical particles, Transp. Porous Media 77 (2008) 17–40.
[36] S.-M. Lee, S.-J.L. Kang, Theoretical analysis of liquid-phase sintering: pore filling theory, Acta mater. 46 (1998) 3191–3202.
[37] T.M. Shaw, Model for the effect of powder packing on the driving force for liquid-phase sintering, J. Am. Ceram. Soc. 76 (1993) 664–670.
[38] F. Delannay, Modelling of the influence of dihedral angle, volume fractions, particle size and coordination on the driving forces for sintering of dual phase systems, Philos. Mag. 85 (2005) 3719–3733.
[39] F. Delannay, C. Colin, On the control of the liquid-phase distribution in multimaterial assemblies processed by liquid-phase sintering, Mater. Sci. Eng. A 495 (2008) 236–243.
[40] F. Delannay, Influence of dihedral angle and grain coordination on densification rate during intermediate and final sintering stages, J. Am. Ceram. Soc. 98 (2015) 3469–3475.
[41] R. Brook, Fabrication[microstructural design] principles for the production of [high density] ceramics with superior mechanical properties, in: Proceedings of the British Ceramic Society,[N-No. 32], 1982, p. 7.
[42] M. Spears, A. Evans, Microstructure development during final/intermediate stage sintering—II. Grain and pore coarsening, Acta Metall. 30 (1982) 1281–1289.
[43] Z.Z. Du, A.C.F. Cocks, Constitutive models for the sintering of ceramic components-I. Material models, Acta Metall. Mater. 40 (1992) 1969–1979.
[44] F. Delannay, Sintering kinetics across pore closure transition accounting for continuous increase in grain coordination with density, J. Am. Ceram. Soc. 98 (2015) 3476–3482.
[45] E.R. Plante, Vapor pressure and heat of sublimation of tungsten, J. Res. Natl. Bureau Stand. A Phys. Chem. 77A (1973) 237–242.
[46] E.L. Cussler, Diffusion Mass Transfer in Fluid Systems, Cambridge University Press, 2009, ISBN 9780521871211.
[47] V. Eremenko, R. Minakova, M. Churakov, Solubility of tungsten in copper-nickel melts, Powder Metall. Metal Ceram. 16 (1977) 283–286.
[48] B. Szpunar, R.W. Smith, A molecular dynamics simulation of the diffusion of the solute (Au) and the self-diffusion of the solvent (Cu) in a very dilute liquid Cu-Au solution, J. Phys. Condens. Matter 22 (2010), 035105 (6pp).